PHYSICAL REVIEW C VOLUME 26, NUMBER 3 SEPTEMBER 1982

Electron-neutrino correlation in the first-forbidden beta decay of ^{11}Be

E. K. Warburton and D. E. Alburger
Brookhaven National Laboratory, Upton, New York 11973

D. H. Wilkinson
Brookhaven National Laboratory, Upton, New York 11973
and University of Sussex, Falmer, Brighton, England

(Received 3 May 1982)

A study of the β-ν angular correlation in the first-forbidden decay of ^{11}Be to the $\frac{1}{2}^-$ 2125-keV level of ^{11}B was performed. The 2125-keV ground-state transition was detected in coincidence with the betas and at 180° to them. The β-ν asymmetry was deduced from the γ-ray Doppler shift. The result obtained as a function of β energy indicates that the β transition is dominated by rank 0 matrix elements and is thus of interest as a test of meson-exchange effects in nuclei. A comparison is made to the large-basis, spurious-free, shell-model predictions of Millener.

[RADIOACTIVITY ^{11}Be from ^{9}Be(t,p): β-γ coin.; plastic and Ge(Li) detectors, measured γ-ray Doppler shift: deduced β-ν asymmetry and rank 0 and 1 contributions to decay to $\frac{1}{2}^-$ state, compared to theory.]

I. INTRODUCTION

The role of pions in nuclei is a subject of extreme importance in nuclear physics and one for which considerable progress in understanding at a fundamental level has been made in recent years. Crucial to further understanding is the provision of more definitive experimental information on pion exchange effects in nuclei.

In a recent review of such effects, Rho and Brown[1] singled out the timelike component of the axial vector current, A_0, as the operator most strongly affected by two-body meson exchange effects. That is, the one-body impulse approximation treatment of the weak interaction in nuclei—such as is operative in normal shell-model calculations—is expected to be strongly modified by pion exchange, particularly one-pion exchange. Since it was first suggested,[2] the large enhancement over the one-body treatment of A_0 brought about by the introduction of meson exchange has been explicitly calculated a number of times. The importance of experimental determinations of phenomena involving this operator is clear.

There are two nuclear processes to which the timelike component of A_0 contributes and from which it appears that experiments can be made with sufficient accuracy to test the effects of pion exchange. One of these is allowed $\Delta T=1$ Gamow-Teller beta decay. The spacelike component of A_0 dominates the decay and the timelike component—often referred to as the first-class induced axial-vector tensor d^I—only enters in the same lower order as the familiar weak magnetism term.[3] However, d^I can be isolated by measuring certain angular correlations (see, e.g., Ref. 4) or by combining precisely measured mirror beta spectra, e.g., $T=1$, $T_Z=\pm 1 \xrightarrow{\beta^{\mp}} T=0$, $T_Z=0$ (see, e.g., Ref. 5).

It is in first-forbidden $J_i \rightarrow J_f$ beta decay (or the inverse μ^- capture) that A_0 has its most dominant role. A_0 is a rank 0 tensor and thus occurs in $\Delta J=0$ transitions only, i.e., if R is the operator rank, then

$$|J_i - J_f| \leq R \leq J_i + J_f \ . \tag{1}$$

For $J_i=J_f=0$ only the two rank 0 one-body operators γ_5 and $\vec{\sigma}\cdot\vec{r}$ are allowed, i.e., the timelike and spacelike components of the axial current, respectively. The relative magnitude of these two matrix elements depends on the energy release and z of the transition and, less sensitively, on the nuclear structure.

In order to extract reliable information on the meson-exchange contribution to A_0 it is necessary

to have a nuclear system for which one-body calculations of A_0 can be carried out to the necessary accuracy. Two cases have been examined so far, namely the decay rates for ^{16}N (Refs. 6 and 7)

$$^{16}\mathrm{N}(0^-;120\ \mathrm{keV})\rightarrow{}^{16}\mathrm{O}(0^+;\mathrm{g.s.})+e^-+\bar{\nu}_e \quad (2a)$$

and ^{18}Ne (Refs. 8 and 9)

$$^{18}\mathrm{Ne}(0^+;\mathrm{g.s.})\rightarrow{}^{18}\mathrm{F}(0^-;1081\ \mathrm{keV})+e^-+\bar{\nu}_e\ . \quad (2b)$$

The mass 16 case has the added feature that the inverse μ^--capture rate has also been determined. Although the present accuracy of these two measured β-decay rates is not as good as desired, there is no doubt that ultimately both can be determined with more than sufficient accuracy for the problem at hand. However, the procedures for *calculating* nuclear matrix elements connecting $1\hbar\omega$ excitations are not as yet fully developed, and in any case are much more subject to the vagaries of nuclear structure than the more usually encountered $\Delta\hbar\omega=0$ phenomena. Thus considerable effort must be spent on calculating the nuclear structure part of these rates as reliably as possible.

Another approach which should be carried on at the same time is to expand as much as possible the number of determinations of A_0. One way to do this is to isolate the rank 0 contribution to $\Delta J=0$, $J_i\neq 0$ first-forbidden beta decays. An attempt to do this theoretically is underway at this laboratory.[10] It is the purpose of this paper to describe an experimental determination of A_0 in such a case.

The beta decay studied was

$$^{11}\mathrm{Be}(\tfrac{1}{2}^+;\mathrm{g.s.})\rightarrow{}^{11}\mathrm{B}(\tfrac{1}{2}^-;2125\ \mathrm{keV})+e^-+\bar{\nu}_e\ . \quad (3)$$

The absolute rate of this β transition has just been redetermined and is known to sufficient accuracy (5%).[11] The problem is to separate the rank 0 and 1 contributions [see Eq. (1)]. This was done by studying the electron-neutrino angular correlation. In the next section we develop the necessary formalism for interpreting this correlation. In Sec. III we describe the experiment. The analysis to extract A_0 is discussed in Sec. IV.

Information serving as background to this paper is given in the preceding general study of ^{11}Be beta decay (Ref. 11), hereafter referred to as I. It is intended that the two papers be read in conjunction.

II. FORMULAS FOR THE ELECTRON-NEUTRINO CORRELATION

A. Origin of the formulas

Expressions for the electron-neutrino angular correlation in first-forbidden beta decay were first calculated correctly in 1953 by Morita[12] and as far as we know have not been utilized previously. We have recast Morita's results in a form more amenable to present use and in doing so have made the same approximations as adopted by Schopper[13] and in I for the first-forbidden β-decay shape factor.

B. Notation

We will use the following notation: $\hbar=m_e=c=1$, $W_0=$ electron end point energy, $W=$ energy of the electron, $\vec{p}=$ electron momentum, $\vec{q}=$ neutrino momentum, $p=(W^2-1)^{1/2}$, $q=W_0-W$, $\theta_{e\nu}=$ angle between $\vec{p}$ and $\vec{q}$, $P_N=$ Legendre polynomial of degree N, $\vec{r}=$ recoiling nucleus momentum, $A=$ recoiling nucleus mass, $E_\gamma=$ γ-ray energy for emission from nucleus with momentum r, and $E_{\gamma 0}=$ γ-ray energy for $r=0$.

C. The formulas

The first-forbidden shape factor, including the electron-neutrino correlation, can be expressed as

$$C(W,\theta_{e\nu})=\sum_{M,N,R} K(MNR)W^M\left[\frac{p}{W}\right]^N P_N(\theta_{e\nu})\ . \quad (4)$$

The maximum value of M is determined by the degree of forbiddenness included in the calculation. The normal approximation corresponding to that given in I is more than adequate for present purposes and limits M to 0, 1, -1, and 2. Note that there is some additional energy dependence contained in $(p/W)^N$ which is factored out for ease of notation and for theoretical reasons. In the same approximation, N takes on the values 0, 1, and 2. $C(W,\theta_{e\nu})$ is linear in the rank R of the interaction because there is no interference between matrix elements of different ranks, only within ranks. In general, R takes on the values 0, 1, and 2 but is subject to the usual limitations due to the initial and final nuclear spins, i.e., Eq. (1). Integration over all possible directions of neutrino emission gives the normal shape factor:

$$C(W)=\int C(W,\theta_{ev})d\Omega_q=\sum_{M,R}K(M0R)W^M . \tag{5}$$

The formalism adopted by Schopper, and in I is

$$C(W)=K(1+aW+b/W+CW^2) . \tag{6}$$

The equivalence to the present notation is

$$K=\sum_R K(00R),\quad Ka=\sum_R K(10R),\ \text{etc} . \tag{7}$$

In Table I we give the $K(MNR)$ to the same order of accuracy (degree of forbiddenness) as Schopper's expressions for the $K(M0R)$. We also use the $\alpha Z \ll 1$ approximation which gives $\mu_1=\gamma_1=\lambda_2=1$ in Morita's expression for $C(W,\theta_{ev})$ and is more than adequate for light ($Z<30$) nuclei. This approximation allows some terms with different μ_1, γ_1, and λ_2 dependences to be collected into a more compact form. The $K(MNR)$ not explicitly given are zero. In Table I the notation of I is used for the nuclear matrix elements (or combinations thereof) ξ_0, w, ξ_1, x, u, and z. Note that ξ_0' and ξ_1' should be understood for ξ_0 and ξ_1.

Equation (4) can be written as

$$C(W,\theta_{ev})=C(W)\left[1+\alpha_1(W)\left[\frac{p}{W}\right]P_1(\theta_{ev})+\alpha_2(W)\left[\frac{p}{W}\right]^2P_2(\theta_{ev})\right], \tag{8}$$

and from Eqs. (4) and (8) the asymmetry coefficient $\alpha_1(W)$, important in the present experiment, is

$$\alpha_1(W)=\sum_{M,R}K(M1R)W^M\Big/\sum_{M,R}K(M0R)W^M . \tag{9}$$

For pure rank 0 ($R0$) decays, e.g., $0^+\leftrightarrow 0^-$, $\alpha_1(W)$ is given by

$$\alpha_1(W;R0)=\frac{\xi_0^2-\frac{1}{9}w^2}{\xi_0^2+\frac{1}{9}w^2-\frac{2}{3}\xi_0 w\cdot\frac{1}{W}} . \tag{10}$$

The normal situation is that $\xi_0^2\gg\frac{1}{9}w^2$ and for all but very small W, we have $\alpha_1(W;R0)\simeq+1.0$, which is the asymmetry coefficient for allowed $R0$ (Fermi) decays. Likewise, the $R0$ contribution to the shape factor $C(W)$ is essentially independent of W except at very small W. For all present purposes then, we can assume $\alpha_1(W;R0)$ to be constant and the $R0$ shape factor to be independent of W.

TABLE I. The $K(MNR)$ coefficients appropriate to the first-forbidden beta decay shape factor $C(W,\theta_{ev})$.

$$C(W,\theta_{ev})=\sum_{M,N,R}K(MNR)W^M\left[\frac{p}{W}\right]^N P_N(\theta_{ev}) .$$

	Rank 0 ($R=0$)		
$N=0$	$K(000)=\xi_0^2+\frac{1}{9}w^2$	$K(-100)=-\frac{2}{3}\xi_0 w$	
$N=1$	$K(010)=\xi_0^2-\frac{1}{9}w^2$		
	Rank 1 ($R=1$)		
$N=0$	$K(001)=\xi_1^2+\frac{1}{18}W_0^2(2x+u)^2-\frac{1}{18}(7u^2+2x^2)$		
	$K(101)=-\frac{4}{3}\xi_1 u-\frac{1}{9}W_0(2x+u)^2$		
	$K(-101)=\frac{2}{3}\xi_1(x+u)$	$K(201)=\frac{1}{18}(10u^2+8x^2)$	
$N=1$	$K(001)=-\frac{1}{3}[\xi_1^2+\frac{4}{3}\xi_1 W_0(2x+u)-\frac{1}{18}W_0^2(2x+u)^2+\frac{1}{2}(2x^2-u^2)]$		
	$K(111)=-\frac{1}{3}[-4\xi_1 u-\frac{2}{3}W_0 u(2x+u)]$		$K(211)=-\frac{1}{3}[2u]^2$
$N=2$	$K(121)=+\frac{1}{9}W_0(4x^2-u^2)$		$K(221)=-\frac{1}{9}[4x^2-u^2]$
	Rank 2 ($R=2$)		
$N=0$	$K(002)=\frac{1}{12}(W_0^2-1)z^2$	$K(102)=-2[\frac{1}{12}W_0]z^2$	$K(202)=+2[\frac{1}{12}]z^2$
$N=1$	$K(012)=-\frac{1}{5}K(002)$	$K(112)=-\frac{6}{5}K(102)$	$K(212)=-\frac{6}{5}K(202)$
$N=2$		$K(122)=\frac{1}{5}K(102)$	$K(222)=\frac{1}{5}K(202)$

The asymmetry coefficient for pure R 1 decays, e.g., $0^+ \leftrightarrow 1^-$, is considerably more complex. Three matrix elements are encountered, and there are interference terms between them. Results for the ^{11}Be(β^-)^{11}B (2125-keV level) will be discussed in Sec. IV.

D. The electron-neutrino asymmetry from the subsequent γ-ray Doppler shift

In the present study information on the electron-neutrino asymmetry, i.e., $\alpha_1(W)$, was determined from the Doppler shift of the 2125-keV γ ray following ^{11}Be β^- decay. In this subsection we consider the relation between this Doppler shift and $\alpha_1(W)$.

In the β decay of a state J_1 to a γ-emitting state J_2, information on the recoil momentum $\vec{r}$ of the nucleus in the state J_2 is contained in the Doppler shift of the subsequent γ transition $J_2 \rightarrow J_3$. This follows from the expression for this Doppler shift, which to first order is

$$\Delta E_\gamma = E_\gamma - E_{\gamma 0} = E_{\gamma 0}\frac{r}{A}\cos\phi \ , \tag{11}$$

where ϕ is the angle between $\vec{r}$ and the direction of emission of the γ ray (see Fig. 1), and the remaining notation is described in Sec. II B. In general, the Doppler shift will depend on the triple correlation of γ-e-ν, but in the present case, with $J^\pi = \frac{1}{2}^-$ for the 2125-keV level and the circular polarization of the γ rays unobserved, the dependence is on the e-ν double correlation aside from terms of order W/A, which are negligbile.

In the present experiment the β and γ rays were emitted in opposite directions as shown in Fig. 1. Neglecting the kinetic energy of the recoiling nucleus [and thus generating errors (negligible) of order W/A]

$$\vec{r} = \vec{p} + \vec{q} \ . \tag{12}$$

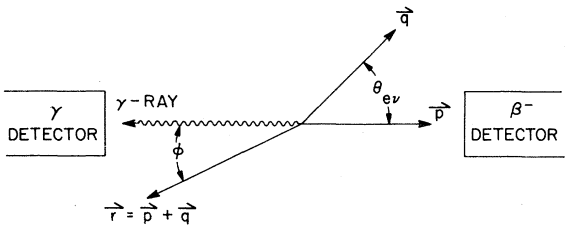

FIG. 1. Geometry for the β-γ coincidence measurement.

We wish to find the average value of ΔE_γ for a given value of W:

$$\frac{A}{E_{\gamma 0}}\langle \Delta E_\gamma \rangle = \frac{1}{p}\langle \vec{r}\cdot\vec{p} \rangle$$

$$= p + (W_0 - W)\langle \cos\theta_{e\nu} \rangle \ , \tag{13}$$

where $\langle\ \rangle$ denotes an average over the direction of emission of the unobserved neutrino. Using Eq. (8) we have

$$\langle \cos\theta_{e\nu} \rangle = \frac{\int \cos\theta_{e\nu} C(W,\theta_{e\nu}) d\Omega}{\int C(W,\theta_{e\nu}) d\Omega}$$

$$= \tfrac{1}{3}\alpha_1(W)\frac{p}{W} \ . \tag{14}$$

Because of the orthonormal properties of the Legendre polynomials, the term in $P_2(\theta_{e\nu})$ does not contribute to $\langle \cos\theta_{e\nu} \rangle$. Finally, from Eqs. (13) and (14) the Doppler shift is

$$\langle \Delta E_\gamma \rangle = \frac{E_{\gamma_0} p}{A}\left[1 + \alpha_1(W)\frac{W_0 - W}{3W}\right] \ . \tag{15}$$

III. EXPERIMENT

A. Design considerations

The aim of the experiment was to determine, in the geometry of Fig. 1, the average Doppler shift of the ^{11}B 2125-keV γ rays in coincidence with those betas from ^{11}Be(β^-)^{11}B feeding the ^{11}B 2125-keV level and as a function of the energy of the betas. Design considerations included: (1) a beta spectrum as free of scattering, energy degradation, random coincidences, pulse pileup, and bremsstrahlung as possible; (2) adequate statistics in the γ detector; and (3) high γ-ray energy dispersion and simultaneous recording of the coincidence matrix and the γ-singles spectrum. Computer simulation indicated that the energy resolution of a plastic scintillator for the beta detection was adequate for our needs. Criterion (3) was met by utilizing the $\Sigma 7$ computer of the BNL MP tandem facility. This demanded signal cables $\sim$160 m long and some loss of γ-ray detector resolution. Because of criterion (2), it was advantageous to use a plastic scintillator for the β detector rather than a magnetic spectrometer. Some effort was then made to determine how well a plastic beta detector met criterion (1).

As a guide to what could be expected for the per-

formance of β-decay detection systems using plastic scintillators, the work of Cramer, Farmer, and Class[14] has shown that remarkably good β spectra (i.e., linear Kurie plots over a wide range of energy) can be obtained with these devices under conditions of good geometry and low scattering. In order to test our overall system and evaluate the quality of the data, measurements were made on the decay of ^{20}F using the Pilot-B beta detector described in I. The same γ detector was used; however, the β absorber in front of the γ detector was reduced to 6.3 mm each of Lucite and brass. ^{20}F is an 11-sec activity which decays $\sim 100\%$ by β rays of $E_{\beta_{\max}} = 5392$ keV to the ^{20}Ne first-excited state at 1634 keV. The activity was made in CaF_2 targets 2 mg/cm^2 thick, deposited on 0.0076-mm thick Ni foil, clamped in a rabbit and bombarded with 2.0-MeV deuterons to form the ^{20}F in the ^{19}F$(d,p)^{20}$F reaction. β-ray spectra were recorded for one half-life of 11 sec in repeated bombard-count cycles and with the beam intensity adjusted to give an initial β-ray counting rate of ~ 18 kHz.

Separate tests were first made by bombarding a target attached to a light aluminum frame, which was then removed from a target chamber, hand carried to the counting station, and measured at a relatively low rate and in a geometry ensuring a small amount of β scattering from neighboring materials. Specific measures of the quality of the data consisted of generating a Kurie plot of the spectrum and evaluating both its linearity and the amplitude of the yield beyond the nominal end point.

Corresponding β-ray spectra of ^{20}F taken with the regular rabbit system described in I and at initial counting rates of 18 kHz showed a deviation of the Kurie plot from linearity much higher in energy and a considerably larger tail of counts beyond the end point as compared with the above test. The poor shape of the Kurie plot was attributed to the scattering of β rays by the stainless steel transfer tubing as well as by the relatively massive rabbit with its metal clamp and screws. In order to reduce the scattering effect noted above, a completely new rabbit system was constructed. The counting station for this is indicated schematically in Fig. 2. Detector positions are those used in the final experiments on ^{11}Be and correspond to half angles of 15° for the detection of both β and γ rays. A tapered brass collimator was used on the β-ray detector to reduce the edge effect of β rays that might pass through or scatter out of the scintillator without losing all of their energy. The 15° half angle was arrived at as a compromise between coincidence yield on one hand and the finite-size effect on the β-γ angular correlation on the other hand. The essential feature of this modified rabbit transfer line was the insertion of a square plastic section 7.5 cm long having walls 1 mm thick and a Mylar window 0.05 mm thick for the emerging β rays. Rabbits were constructed of Delrin but with ends and a cross piece only 1 mm thick and with the target cemented across a hole in the cross piece. Thus, there were no screws or other metal parts within 3.7 cm of the target spot and a minimum of plastic materials near the target. Analysis of the ^{20}F β-ray spectrum recorded under these conditions showed no discernible differences with that measured for the initial test described above.

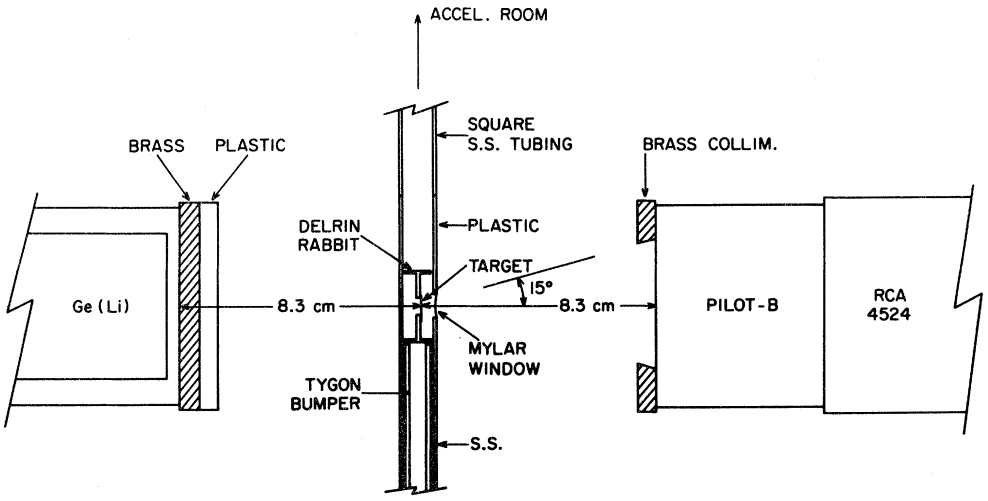

FIG. 2. Schematic of the β-γ detection system.

The best compromise between reduction of random coincidences and pulse pileup on one hand and β energy resolution and linearity on the other was obtained by sending the fast ($\sim$50 nsec) pulses from the photomultiplier base to an ORTEC 460 delay-line amplifier, modified for a shaping time constant of 0.2 μsec, and thence to an ORTEC 474 timing filter amplifier, and finally an ORTEC 442 linear gate and stretcher. The last of these was set to give output pulses 0.6 μsec in duration for connection to the analog-to-digital convertor (ADC) of the Σ7 computer.

Figure 3(a) shows the ^{20}F β-ray singles spectrum recorded at the rate used in the subsequent ^{11}Be experiments, i.e., an initial rate of $\sim$18 kHz. On the right is a plot of the end-point region on an expanded vertical scale illustrating the sum of pulse pileup and real β-γ summing beyond the β end point. β rays in coincidence with the photopeak of the 1634-keV γ rays as recorded in the Ge(Li) detector are shown in Fig. 3(b) and the Kurie plot of this spectrum is given in Fig. 3(c). The latter shows acceptable linearity above 1.8 MeV, i.e., $\frac{1}{3}E_{\beta_{\max}}$.

Other tests on the system consisted of measuring γ-ray spectra in the β-ray detector by covering it with a 9-mm thick brass plate to exclude all β rays. This was done for both ^{20}F and ^{11}Be and was important for the ^{11}Be analysis because of the presence of γ rays extending up to 8 MeV in energy. Energy calibration of the β detector was made from Kurie plots of ^{28}Al, ^{20}F, and ^{11}Be β spectra and from γ-ray spectra from ^{28}Al, ^{20}F, ^{11}Be, ^{137}Cs, ^{88}Y, ^{22}Na, and ^{228}Th. The energies associated with the γ-ray Compton edges were computed using the procedures developed by Cramer *et al.*[14] The energy versus pulse-height curve for the β detector was found to be linear but with a nonzero intercept. The response of the β detector to monoenergetic electrons and its energy resolution were measured using a ^{207}Bi conversion electron source. The pulse response was found to be dominated by a symmetric peak which was well described by a Gaussian and which had an energy resolution (FWHM) at 1.06 MeV of 13.9%. In subsequent analysis the energy resolution of this peak was assumed to vary as $E_\beta^{1/2}$. In addition there was some low energy tailing. The shape and magnitude of this tail were not accurately determined by the ^{207}Bi spectrum. It was assumed to be a constant intensity plateau extending to zero energy and with a total intensity (7 ± 3)% of the intensity in the Gaussian, independent of beta energy. The shape and magnitude of this low-energy tail are in rough agreement with that expected for the back-

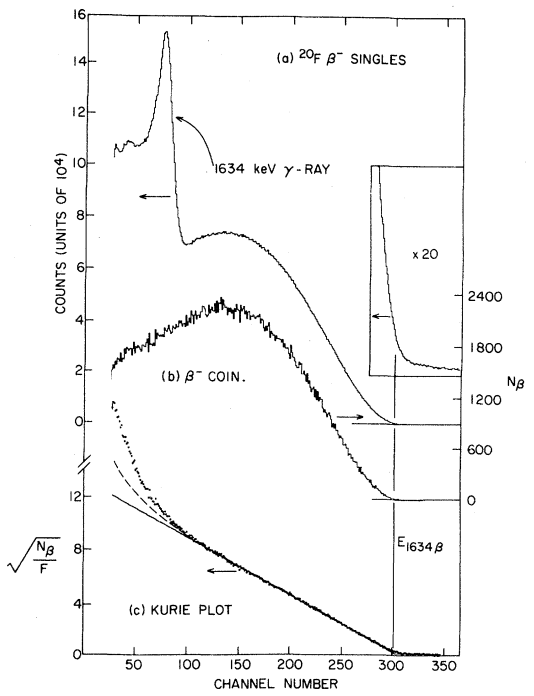

FIG. 3. Beta spectra from ^{20}F(β^-)^{20}Ne (1634-keV level). The original data (2048 channels) have been compressed by a factor of 4 and the nonzero intercept has been subtracted. The singles spectrum (a) contains a contribution from the Compton distribution of 1634-keV γ rays in the plastic scintillator and from β-γ summing which is apparent beyond the end point (see insert). These two contributions are absent in the spectrum (b) of betas in coincidence with the full-energy peak of the 1634-keV γ ray. The Kurie plot (solid curve) for the allowed decay of (b) is linear down to $E_\beta \simeq 1.8$ MeV; the end point, labeled E_{1634}, is 5392 keV. The dotted curve shows the effect on the Kurie plot of the beta response function as described in the text.

scattering of electrons from the plastic scintillator.[15] As a consistency check, this response function was folded into the theoretical ^{20}F beta spectrum. The resulting Kurie plot is illustrated by the dotted curve in Fig. 3(c). The finite resolution nicely reproduces the curvature of the data near the end point (not readily apparent in the figure) and obviously explains some of the curvature below channel 100. However, although not apparent in the scale of Fig. 3(c), this response function produces more curvature above channel 100 than is indicated by the data. Thus, we consider the effect of the assumed tail in the energy region above channel 100 to be an upper limit to any actual scattering effects.

While the ^{20}F activity served to check various as-

pects of the exprimental setup, electronics, and data quality, it unfortunately could not be used to test the γ-ray Doppler shift versus β-ray energy to be measured in the ^{11}Be case. Because of the relatively long lifetime of the ^{20}Ne 1634-keV level ($\tau = 1.05 \pm 0.06$ psec) (Ref. 16), the ^{20}Ne nucleus from the ^{20}F β decay slows down before the 1634-keV γ ray is emitted, thereby, to a large extent, attenuating the Doppler effect. This is not the case for the ^{11}Be β decay since the mean lifetime of the 2125-keV state in ^{11}B is only 5.1 ± 0.4 fsec.[16] However, even in this case a small correction for the lifetime must be made, as described later.

B. The measurement

After the initial tests, final measurements of the ^{20}F β-γ and ^{11}Be β-γ coincidences of 50 and 63 h duration were made in the geometry of Fig. 2. The coincidence data were recorded on magnetic tape in an EMR $2048(\beta) \times 8192(\gamma)$ matrix for later analysis. The coincidence time resolution was ~ 10 nsec. The ^{11}Be counting cycle was as in I with initial β- and γ-counting rates of ~ 18 and 6 kHz, respectively. The γ spectra were collected with an energy dispersion of 0.318 keV/channel.

The ^{11}Be beta spectra of Fig. 4 are similar to the ^{20}F spectra of Fig. 3. Figure 4(a) shows the singles spectrum collected simultaneously with the coincidence data. The spectrum of Fig. 4(b) is in coincidence with the ^{11}B 2125-keV full-energy-loss peak, and Fig. 4(c) displays the Kurie plot corresponding to Fig. 4(b).

The theoretical calculations of I and the results of the present experiment lead us to expect a quite small deviation from the allowed shape for the ^{11}Be$(\beta^-)^{11}$B branch to the 2125-keV level. The results for ^{20}F [shown in Fig. 3(c)] lead us to expect discernible effects of scattering, etc., only below a β

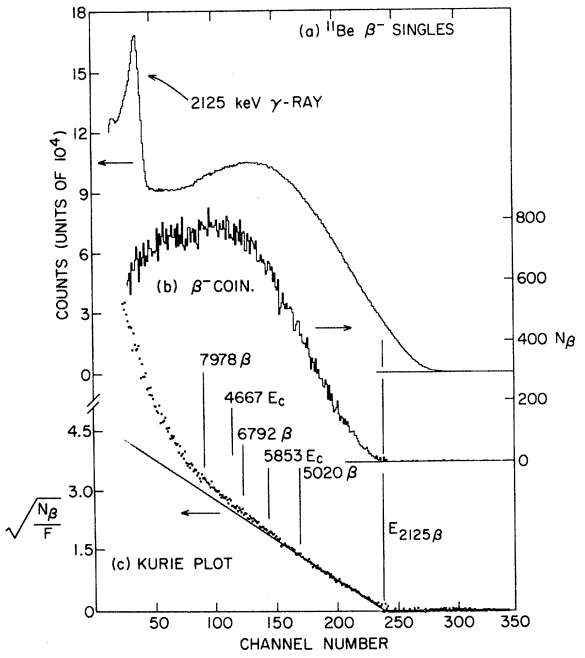

FIG. 4. Beta spectra from ^{11}Be$(\beta^-)^{11}$B. The decay is complex. For instance, the branch to the ^{11}B g.s. is evident from a comparison of (a) and (b); and the β or γ components with end points (β) or Compton edges (E_c) are expected as marked in (c) which is a Kurie plot of (b). See the caption of Fig. 3 and Table II for other details.

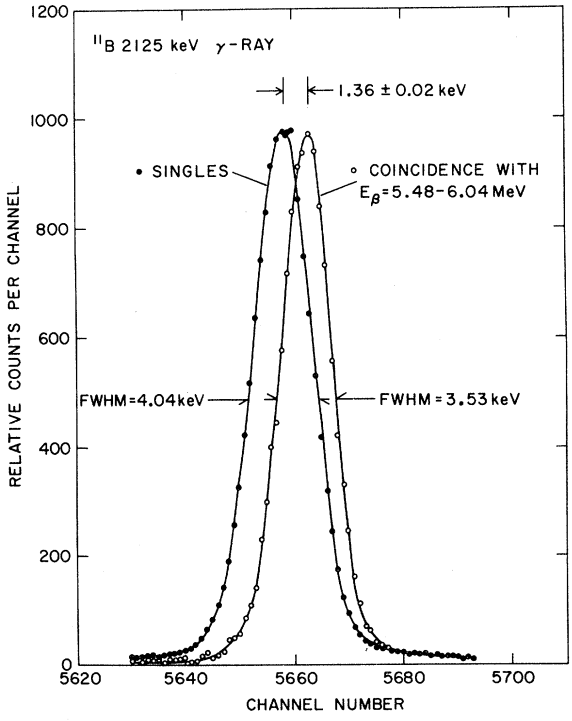

FIG. 5. The full-energy peak of the ^{11}B 2125-keV γ observed in ^{11}Be$(\beta^-)^{11}$B. The singles and coincidence data were stored simultaneously. The coincidence data were analyzed into 16 γ spectra associated with equal energy segments of the beta spectrum of Fig. 4(b). The coincidence peak shown is one of these spectra. The separation of 1.36 ± 0.02 keV for the two peaks shown is the centroid separation determined from a peak and background fitting routine.

energy between ~ 1.8 MeV and $\frac{1}{3}E_{\beta_{max}}$ ($\frac{1}{3}9.383 = 3.13$ MeV). Thus, the deviation from the Kurie plot above channel 80 in Fig. 4(c) is attributed almost entirely to the β spectra and γ Compton distributions identified in the figure. These contributions are due to real coincidences with the 2125-keV γ ray as expected from the known decay scheme (see Fig. 1 of I). The correction for their presence is described in the next subsection.

Analysis started by dividing the β^- coincidence spectrum of Fig. 4(b) into 16 equal energy bins and displaying the γ spectra in coincidence with each. In Fig. 5 the 2125-keV full-energy peak in coincidence with one of the bins is compared to the peak observed in singles. Both peaks are broadened by Doppler effects. The actual detector resolution at $E_\gamma = 2$ MeV was 3.18 keV full width at half maximum (FWHM). The centroid of the 2125-keV peak in the 16 coincidence spectra and in singles was determined using several different fitting procedures. The differences were not important. The results (solid black points) are shown as a function of β energy in Fig. 6. There are several corrections to be made to these data. These corrections we now consider.

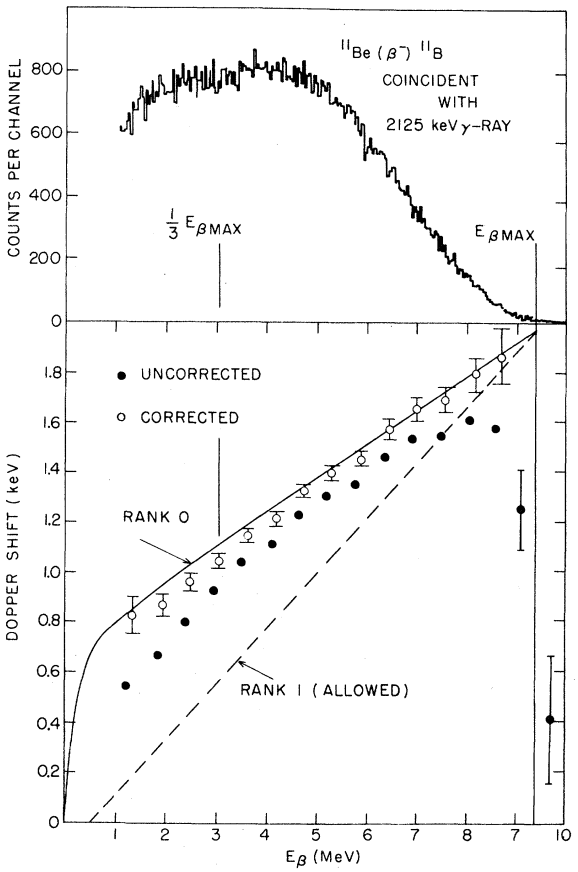

FIG. 6. The Doppler shift of the 2125-keV γ ray from ^{11}Be(β^-)^{11}B as a function of E_β. The original data, e.g., that of Fig. 5, are given by the solid points. The open circles represent the data after correction for various effects as explained in the text. The solid curve is the expected Doppler shift for pure rank 0 decay, either allowed or first-forbidden. The dashed curve is that expected for rank 1 allowed decays, i.e., $\alpha_1(W) = -\frac{1}{3}$. This latter curve is shown since it is used in the correction for the presence of allowed decays to the ^{11}B 6792- and 7978-keV levels.

C. Corrections to the data

Effects which were considered as possibly influencing the Doppler shift data were the following:

(i) real coincidences with β branches to higher-lying ^{11}B levels which subsequently decay partially to the 2125-keV level;

(ii) Doppler shift attenuation of the ^{11}B recoils in the ^{9}Be target;

(iii) the finite size of the β and γ detectors;

(iv) bremsstrahlung from interactions outside the β detector with subsequent detection of the radiation in the β detector;

(v) bremsstrahlung in the β detector with escape of the radiation;

(vi) the finite beta energy resolution and bin size;

(vii) pulse pileup of coincidence betas with betas (singles) and random β-γ coincidences;

(viii) the effect of the low-energy tail in the beta response function;

(ix) the uncertainty in the beta energy calibration.

We consider these corrections in turn:

(i) From the ^{11}Be decay scheme (Table I of I) the relative intensities of the β and γ transitions which are in coincidence with the 2125-keV β ray are calculated to be in the ratio given in Table II. In addition to the four β^- distributions with end points as marked in Fig. 4(c), the 2895-, 4666-, and 5851-keV

TABLE II. Relative intensities of the four ^{11}Be β^- distributions in coincidence with the ^{11}B 2125-keV γ ray.

^{11}B γ ray (keV)	Originating ^{11}B level (keV)	β^- end point (keV)	Relative intensity (%)
2125	2125	9383	89.8
2895	5020	6488	0.10
2895	6792	4716	0.10
4666	6792	4716	4.59
5851	7978	3530	5.39

γ rays are in coincidence with the 2125-keV γ ray and so are detected in the β detector via the Compton process. The effect of the branch to the 5020-keV level is negligible. The other two higher branches are allowed, i.e., Gamow-Teller transitions of rank 1. For these the electron-neutrino asymmetry coefficient is therefore $\alpha_1=-\frac{1}{3}$ independent of energy[13] and so the correction to the Doppler shift for these higher-lying branches is readily made utilizing the measured response of the β detector to γ rays. The Doppler shift corresponding to $\alpha_1=-\frac{1}{3}$ is illustrated by the dashed curve in Fig. 6.

(ii) There is some diminution of the recoiling ^{11}B velocity and thus of the Doppler shift during the finite lifetime of the 2125-keV level. This effect was calculated using the approach of Blaugrund[17] including an estimate of the approximation $\langle v\cos\phi\rangle=v\langle\cos\phi\rangle$.[17,18] For the small velocities encountered in beta recoils, the phenomenological expression used by Blaugrund for the nuclear stopping power $(d\epsilon/d\rho)$ is not adequate. We have used a later expression, due to Oetzmann,[19] which reproduces a large body of experimental data within a maximum deviation of 15%,

$$(d\epsilon/d\rho)_n=\frac{1.7\epsilon^{1/2}\ln(\epsilon+e)}{1+6.8\epsilon+3.4\epsilon^{3/2}}\ . \tag{16}$$

The diminution is a function of the initial recoil velocity which is given by

$$r^2=p^2+q^2+2pq\cos\theta_{e\nu}\ . \tag{17}$$

The average value of r for a given beta energy W is obtained by substituting $\langle\cos\theta_{e\nu}\rangle$ from Eq. (14) for $\cos\theta_{e\nu}$ in Eq. (17). This value was used in calculating the correction for a given W. Using 5.1 ± 0.4 fsec for the mean life of the 2125-keV level, the diminution of the Doppler shift was calculated to vary between 3 and 4% with a maximum near $W=W_0/2$. The data points were adjusted accordingly, and a 20% uncertainty was assigned to this correction.

(iii) The finite size correction is easily made for the cylindrical geometry used. We chose to correct the theoretical distributions rather than experiment. This is done by multiplying $\alpha_1(W)$ in Eq. (9) by $Q_1^\beta Q_1^\gamma=0.9633$, where Q_1 is the standard attenuation coefficient.[20]

(iv) Both bremsstrahlung effects [corrections (iv) and (v)] were calculated in some detail utilizing numerical integration. The external effect was calculated with the brass collimator as the sole radiator. The contribution to the β spectrum with $E_{\beta_{\max}}=9383$ keV was found to decrease rapidly with increasing energy and to be negligible ($<0.4\%$) for $E_\beta>3$ MeV.

(v) Escape of bremsstrahlung from the detector results in an effective lowering of the beta energy so that the Doppler shift in coincidence with a given β-energy bin will contain some contribution from higher-energy betas. The effect on the Doppler shift was calculated as a function of β energy. At $E_\beta=3$ MeV the effect is ~15 eV and falls with increasing E_β. This almost negligible correction was made.

(vi) These two effects are similar. They were calculated by numerical integration and the almost negligible correction was made.

(vii) Estimates from the observed rates and resolving times and various tests with variable counting rates and source-detector distances indicated that the effects of pulse pileup and random coincidence were comparable. The exact balance was hard to ascertain within a factor of 2. Thus, the correction for the two effects contains an uncertainty due to that in the balance. As for the magnitude of the combined effect, this was assumed to give rise to the excess pulses above $E_{\beta_{\max}}$ other than those due to the finite resolution. The biggest uncertainty in this correction was due to the uncertainty in the pileup spectrum due to the unknown relationship between the rise time of the beta pulses and the effective pileup resolving time.

The theoretical Doppler shift at $E_{\beta_{\max}}$ is independent of $\alpha_1(W)$ since the neutrino momentum is here zero and just below $E_{\beta_{\max}}$, the Doppler shift is insensitive to $\alpha_1(W)$. This is true for first-forbidden decays as well as the theoretical Doppler shifts shown in Fig. 6 for allowed decays. The two effects of pileup and accidentals are responsible for the rapid falloff of the measured Doppler shift near and just above $E_{\beta_{\max}}$ as shown in Fig. 6. Thus, a check on the correction for these effects is that the last three points end up near the calculated shift. This was indeed the case. Because of excessive uncertainties in this correction the two highest energy points were discarded. The correction to the remaining points varied from 14% for the highest energy point retained to 1% at $E_\beta=5$ MeV. The estimated uncertainty on the correction was 40%.

(viii) The low-energy tail to the beta response function was described in Sec. III A. The correction to the Doppler shift for this tailing was evaluated by numerical integration. For a 7% intensity tail the correction varied from -60 to -3 eV for E_β varying from 2.3 to 8.0 MeV. A 40% uncertainty was assigned to this correction.

(ix) The least squares fit to the beta calibration

energies as described in Sec. III A also yielded the uncertainty in E_β as a function of channel number. The uncertainty varied linearly from 35 keV at $E_\beta=0$ to 108 keV at the end point. This translates into an uncertainty in the Doppler shift varying essentially linearly from 6 to 15 eV from $E_\beta=1$ to 9.4 MeV.

The corrected Doppler shift data are shown by the open circles in Fig. 6. The error bars for $E_\beta>3$ MeV include all known sources of uncertainty; as E_β falls below 3 MeV, the effects of scattering, source thickness, bremsstrahlung, etc., are increasingly important and have not been corrected for to the extent that the finite resolution Kurie plot of Fig. 3(c) fails to reproduce the data. In the next section we will compare the corrected results to expectations for first-forbidden decay.

IV. ANALYSIS

The corrected Doppler shift data are again shown in Fig. 7. Here the comparison is to various predictions for the first-forbidden decay $^{11}\mathrm{Be}(\frac{1}{2}^+)\rightarrow{}^{11}\mathrm{B}(\frac{1}{2}^-)$. We shall consider only the energy region labeled as the region of reliability in Fig. 7. It is here that the statistical errors are at a minimum and the composite of the various corrections is most reliable.

Since there is no interference between matrix elements of different ranks, the analysis of Fig. 7 proceeds formally by calculating the $R0$ and $R1$ results and combining them via

$$\alpha_1(W)=\frac{\alpha_1(W;R0)+RC(W)\cdot\alpha_1(W;R1)}{1+RC(W)}\,, \tag{18}$$

where $RC(W)$ is the ratio of the $R1$ and $R0$ parts of the shape factor $C(W)$ of Eq. (5).

As defined in Eqs. (14)–(16) of I there are actually eight matrix elements contributing to the $^{11}\mathrm{Be}(\frac{1}{2}^+)\rightarrow{}^{11}\mathrm{B}(\frac{1}{2}^-)$ beta decay. However, w', x' and u' are closely related to w, x, and u and can be taken as proportional to them. This leaves the two $R0$ matrix elements $\xi' v$ and w and the three $R1$ matrix elements $\xi' y$, x, and u. Our measurement cannot determine $\xi' v$ and w separately, only the combined $R0$ contribution. The relation between $\xi' y$ and x is fixed by the conserved vector current (CVC) (see I). Thus, there are essentially three independent variables entering in the behavior of $\alpha_1(W)$.

The analysis to extract the relative $R0$ and $R1$ matrix elements makes strong use of the insensitivity of the $R0$ asymmetry to the relative values of the $R0$ matrix elements. In the region of reliability of Fig. 7, $\alpha_1(W;R0)$ deviates $<1.0\%$ from $+1.0$; this deviation is quite insensitive to the relative values of the two $R0$ matrix elements $\xi' v$ and w. For all practial purposes, then, $\alpha_1(W;R0)$ can be considered as a constant independent of W and nuclear structure.

The asymmetry for $R1$ is quite different. First of all, $\alpha_1(W;R1)$ is strongly dependent on the relative signs and magnitudes of the three matrix elements, $\xi' y$, x, and u (see I) that contribute. Second, $\alpha_1(W;R1)$ is strongly sensitive to W_0 and z. This sensitivity comes mostly through interference terms. Since the relationship between $\xi' v$ and x is fixed, we need only consider the effect on $\alpha_1(W;R1)$ of the relative values of x and u. This effect is illustrated for the $^{11}\mathrm{Be}(\frac{1}{2}^+)\rightarrow{}^{11}\mathrm{B}(\frac{1}{2}^-)$ transition in Fig. 8. The $u=0$ curve shows $\alpha_1(W;R1)$ calculated for $\xi' y$ and x only. Its value is dominated by the interference terms between $\xi' y$ and x which are fixed by CVC and the values of W_0 and z appropriate to the transition. In the high-energy limit, x dominates $\xi' y$ and $\alpha_1(W;R1)$ for $u=0$ and $W_0\rightarrow\infty$, has the value $+1$ at $W=1$, increases to $+1.5$ at $W=W_0/2$, and falls symmetrically to $+1$ at $W=W_0$. For $x=\xi' y=0$, $\alpha_1(W;R1)$ for $^{11}\mathrm{Be}(\frac{1}{2}^+)\rightarrow{}^{11}\mathrm{B}(\frac{1}{2}^-)$ is as shown for the $x=0$ curve of Fig. 8. The $x=0$ value of $\alpha_1(W;R1)$ is much less sensitive to W_0 than the $u=0$ value of $\alpha_1(W;R1)$. For instance, in the high-energy limit,

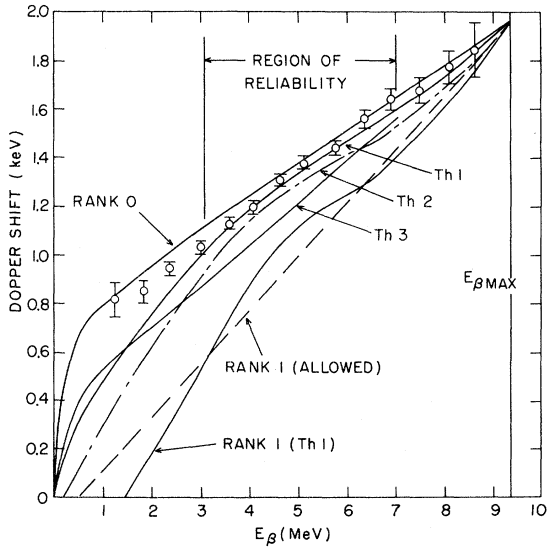

FIG. 7. The corrected Doppler shift data of Fig. 6. The theoretical curves labeled Th1, Th2, and Th3 are explained in the text.

the $x=0$ curve of Fig. 8 has the values -1 at $W=1$ and $W=W_0$ and 0 at $W=W_0/2$ and is symmetric about $W_0/2$. This is not too different from the $x=0$ curve of Fig. 8. The curves labeled Th1 and Th2 in Fig. 8 will be explained below. They are calculated from nonzero values of $\xi' y$, x, and u.

To illustrate this calculation we start with the theoretical value of u $(=1.387)$ appropriate to the $0\hbar\omega$, harmonic oscillator value and the value of x $(=0.163)$ corresponding to the measured $B(E1)$ for the analog $^{11}\mathrm{B}(\frac{1}{2}^+)\rightarrow{}^{11}\mathrm{B}(\frac{1}{2}^-)$ γ decay (see column one, Table VIII of Ref. 1). These values are labeled $u(\mathrm{Th1})$ and $x(E1)$. The sign of x is taken from the Th1 calculation. These values result in the curves marked Th1 in Figs. 7 and 8, give $f^{(1)}=24$, and hence $f^{(0)}=140-24=116$, and result in a satisfactory fit to the data. The curve marked Th2 in Fig. 7, corresponds to $x(E1)$, $\sqrt{2}\,u(\mathrm{Th1})$ and Th3 corresponds to $3\cdot x(E1)$, $u(\mathrm{Th1})$. The $\alpha_1(W;R1)$ for this latter case is also shown in Fig. 8. Perusal of the curves Th1, Th2, and Th3 in Fig. 7 shows that the Doppler shift is sensitive to x and u in different regions of W. Roughly speaking, u dominates x $(f^{(1)}=24$ and 23 for Th1 and $x=0$, respectively), and the relative intensities of $\alpha_1(W;R0)$ and $\alpha_1(W;R1)$ are sensitive to u, while the sensitivity to x comes through the u-x interference which causes the differences between the $x=x(E1)$ and $x=3\cdot x(E1)$ curves in Fig. 8.

From a detailed consideration of the variation of x and u we conclude

$$|x|<2|x(E1)|;\quad |u|<\sqrt{1.5}\,|u(\mathrm{Th1})|\ , \tag{19}$$

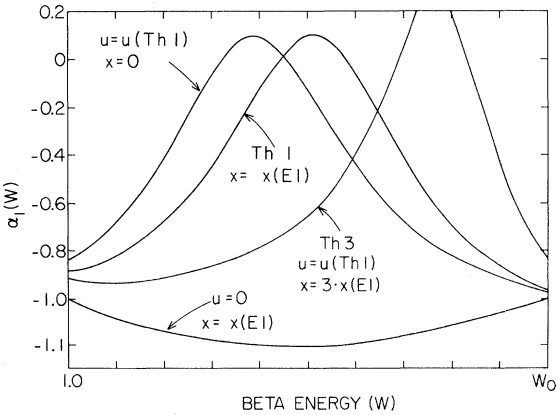

FIG. 8. The electron-neutrino angular correlation asymmetry $\alpha_1(W)$ for the rank 1 part of the $^{11}\mathrm{Be}(\frac{1}{2}^+)\rightarrow{}^{11}\mathrm{B}(\frac{1}{2}^-)$ beta decay. The various curves are discussed in the text. Those labeled Th1 and Th3 are related to those similarly labeled in Fig. 7.

where $x(E1)=0.164$ and $u(\mathrm{Th1})=1.387$. Also

$$f^{(1)}<33;\quad f^{(0)}=115\pm18\ . \tag{20}$$

The limtis on x and u and $f^{(1)}$ are for the case when x and u have the same sign, as considered here. This is the "worst" case since for these signs x and u have destructive interference. For opposite signs the limits would be somewhat more severe.

V. CONCLUSIONS

We set out to separate as far as possible the $R0$ and $R1$ contributions to $^{11}\mathrm{Be}(\frac{1}{2}^+)\rightarrow{}^{11}\mathrm{B}(\frac{1}{2}^-)$ beta decay. The method used was a determination of the electron-neutrino angular correlation asymmetry coefficient. The attempt was successful in that the $R0$ decay rate was determined to $\sim15\%$, an accuracy competitive with that achieved in other light $(A<30)$ nuclei. Some information was also obtained on the individual contributions of the $R1$ matrix elements.

In their theoretical study of first-forbidden nonunique beta transitions in light nuclei, Towner and Hardy[21] found rather small deviations of the beta spectrum from the allowed shape. The reason for this was that the three cases they considered were all $\frac{1}{2}^{\pm}\rightarrow\frac{1}{2}^{\mp}$ transitions for which the $R0$ contribution was dominant and the $R0$ contribution had, apart from a negligible W^{-1} term, an allowed shape. The present results indicate that measurement of the asymmetry $\alpha_1(W)$ provides a more sensitive determination of the matrix elements contributing to the decay than does a measurement of $C(W)$. However, it may be that useful limits on the contribution of $R1$ to these decays could be set from a careful examination of the energy dependence of the shape factor.

The shell-model calculations of x and u (and thus $f^{(1)}$) described in I are relatively insensitive to the radial wave functions and to inclusion of $2\hbar\omega$ terms. They give $x\simeq0.45$ and $u\simeq1.4$. The present experiment results in the limits $x<0.33$ and $u<1.7$. The disagreement for x is not significantly severe to be informative.

The rank-zero contribution to the $\frac{1}{2}^+\rightarrow\frac{1}{2}^-$ beta decay was found to be $f^{(0)}=115\pm18$. As discussed in I, this parameter places severe constraints on the mass 11 wave functions. It is not possible to reproduce it with harmonic-oscillator radial wave functions. Use of the more realistic Woods-Saxon wave functions gives a dramatic improvement in the agreement. Inclusion of $2\hbar\omega$ admixtures in the predominant $0\hbar\omega$ $^{11}\mathrm{Be}$ ground-state wave function

also helps agreement. Because of the sensitivty of the calculation to the radial wave functions and $2\hbar\omega$ component of the $^{11}\mathrm{B}\ \frac{1}{2}^-$ state, the calculation can also be made to reproduce $f^{(0)}=115$ with $\sim 40\%$ meson exchange effects with reasonable changes in the wave function. The situation is summarized by Eq. (23a) of I rewritten as

$$f^{(0)} \cong 0.678[(\mathrm{MEC})\xi' v + 7.79w]^2 , \tag{21}$$

where (MEC) represents the meson exchange enhancement factor. Inserting the value of w found for the $0\hbar\omega$ calculation with Woods-Saxon radial wave functions, $w=-1.182$, and setting the right side of Eq. (21) equal to 115, we find

$$(\mathrm{MEC})\xi' v \simeq 22.2 . \tag{22}$$

Thus, for a predicted MEC enhancement factor of ~ 1.4, we would have $\xi' v \simeq 15.9$, which is $\sim 71\%$ of the calculated value. Such a change is realizable with reasonable changes in the parameters of the model. Thus, it is not possible to draw any conclusions about any MEC enhancements from the present comparison. Rather the need for the omnibus comparison referred to in the Introduction is reinforced.

ACKNOWLEDGMENTS

We would like to thank D. J. Millener for many enlightening discussions and for the use of his theoretical calculations. This research was supported by the U. S. Department of Energy, Division of Basic Energy Sciences, under Contract No. DE-AC02-76CH00016.

[1]M. Rho and G. E. Brown, Comm. Nucl. Part. Phys. A 10, 201 (1981).
[2]K. Kubodera, J. Delorme, and M. Rho, Phys. Rev. Lett. 40, 755 (1978).
[3]B. R. Holstein, Rev. Mod. Phys. 46, 789 (1974).
[4]H. Brändle *et al.*, Phys. Rev. Lett. 41, 299 (1978); Y. Masuda *et al., ibid.* 43, 1083 (1979).
[5]F. P. Calaprice, W. Chung, and B. H. Wildenthal, Phys. Rev. C 15, 2178 (1977).
[6]L. Palffy, J. P. Deutsch, L. Grenacs, J. Lehmann, and M. Steels, Phys. Rev. Lett. 34, 212 (1975).
[7]I. S. Towner and F. C. Khanna, Nucl. Phys. A372, 331 (1981).
[8]E. G. Adelberger, C. D. Hoyle, H. E. Swanson, and R. D. Von Lintig, Phys. Rev. Lett. 46, 695 (1981).
[9]W. C. Haxton, Phys. Rev. Lett. 46, 698 (1981).
[10]D. J. Millener and E. K. Warburton (unpublished).
[11]D. J. Millener, D. E. Alburger, E. K. Warburton, and D. H. Wilkinson, Phys. Rev. C 26, 1167 (1982). Hereafter referred to as I.
[12]M. Morita, Prog. Theor. Phys. (Tokyo) 9, 345 (1953).
[13]H. Schopper, *Weak Interactions and Nuclear Beta Decay* (North-Holland, Amsterdam, 1966).
[14]J. G. Cramer, B. J. Farmer, and C. M. Class, Nucl. Instrum. Methods 16, 289 (1962).
[15]W. Paul and H. Steinwedel, *Beta- and Gamma-Ray Spectroscopy,* edited by Kai Siegbahn (North-Holland, Amsterdam, 1955), Chap. I.
[16]F. Ajzenberg-Selove, Nucl. Phys. A300, 1 (1978); F. Ajzenberg-Selove and C. L. Busch, *ibid.* A336, 1 (1980).
[17]A. E. Blaugrund, Nucl. Phys. 88, 501 (1966).
[18]W. M. Currie, Nucl. Instrum. Methods 73, 173 (1969).
[19]H. Oetzmann, Inaugural dissertation, University of Heidelberg, 1976.
[20]J. B. Marion and F. C. Young, *Nuclear Reaction Analysis* (North-Holland, Amsterdam, 1968), pp. 70–71.
[21]I. S. Towner and J. C. Hardy, Nucl. Phys. 179, 489 (1972).